Bioconjugate Chemistry

Article

pubs.acs.org/bc

Construction of a Ca^{2+}-Gated Artificial Channel by Fusing Alamethicin with a Calmodulin-Derived Extramembrane Segment

Daisuke Noshiro, Kazuhiro Sonomura, Hao-Hsin Yu, Miki Imanishi, Koji Asami, and Shiroh Futaki*

Institute for Chemical Research, Kyoto University, Uji, Kyoto 611-0011, Japan

Supporting Information

ABSTRACT: Using native chemical ligation, we constructed a Ca^{2+}-gated fusion channel protein consisting of alamethicin and the C-terminal domain of calmodulin. At pH 5.4 and in the absence of Ca^{2+}, this fusion protein yielded a burst-like channel current with no discrete channel conductance levels. However, Ca^{2+} significantly lengthened the specific channel open state and increased the mean channel current, while Mg^{2+} produced no significant changes in the channel current. On the basis of 8-anilinonaphthalene-1-sulfonic acid (ANS) fluorescent measurement, Ca^{2+}-stimulated gating may be related to an increased surface hydrophobicity of the extramembrane segment of the fusion protein.

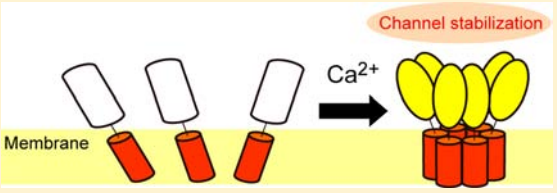

INTRODUCTION

Artificial channel construction is gaining popularity and could ultimately lead to the development of molecular and nanosensing devices.[1−3] The resulting insights may aid in the design of other membrane proteins and receptors to analyze and control cellular functions. Successful approaches that employ membrane proteins containing a membrane-spanning pore for the construction of artificial channels have been reported. Many of these studies have focused on the design or modification of the channel pore and the channel entrance for the detection of specific ions or analytes, including DNAs, that go through the channel pores.[4] Alternative approaches have demonstrated the creation of artificial channels using self-assembling transmembrane peptides.[5,6] Since alterations in association states can influence the ion flux through channel pores, channel gating by controlling the assembly of channel-forming peptides is therefore possible.

Ca^{2+} has an important physiological role as a ubiquitous intracellular mediator.[7] Intracellular Ca^{2+} concentrations are mediated by various Ca^{2+} channels, pumps, and transporters.[8] Manifesting the fundamental properties that characterize natural Ca^{2+}-gated channels (i.e., Ca^{2+}-binding and resulting channel opening) using a simplified structure is thus a challenge and an attractive target in molecular and functional design considering the potential applications to channel-based artificial sensors/devices. This system may also be employable to synthetic biological studies to construct artificial cells.[9]

Alamethicin (Alm) is an antimicrobial peptide that self-assembles in membranes to form ion channels[10] and has often been employed as a framework for artificial ion channels. For example, we reported that disposition of a His residue on the N-terminus of Alm led to the stabilization of Alm assembly in the membranes by divalent metal ions including Zn^{2+} and thus yielded metal-sensitive channels.[11] Woolley et al. previously constructed an Alm-based artificial channel bearing a pyromellitate moiety on the C-terminus (Alm-PM) that was activated by Ca^{2+}.[12] The gating mechanism of this channel is proposed to be the cancellation of electrostatic repulsion between the pyromellitate moieties by Ca^{2+}, which facilitates self-association of Alm-PM to form channels in lipid bilayers. This observation elegantly exemplifies the design concept of gating channels and is an important advancement in the research field; however, the pyromellityl group was not optimized for Ca^{2+} binding. Therefore, the specificity to Ca^{2+} for the gating may not necessarily be high.

The extramembrane domain of a channel is also important as a functional unit for ligand interaction and gating,[13−15] as is seen in natural channel proteins. Natural Ca^{2+}-gated K^+ channels open in response to Ca^{2+} binding through conformational changes of the extramembrane domain interfaces in the intracellular compartment.[16] We have reported the creation of a simplified Alm-based ligand-gated ion channel using Fe(III) as a model ligand. In this channel, Fe(III)-stimulated conformational alterations in its extramembrane segments are transmitted to the transmembrane segments, leading to an increase in channel current (ion flux).[15] The concept of channel gating by extramembrane conformational alterations that affect the association state of the transmembrane segments should provide a promising approach for the design of sensing devices for specific ligands. However, in the case of the above Fe(III)-gated channels, a pair of iminodiacetic acid moieties were introduced in the extramembrane segment to attain a conformational change by complex formation with Fe(III). If we utilize natural protein motifs specific to intrinsic ligands as an extramembrane segment, more sophisticated channels

Received: August 25, 2012
Revised: December 20, 2012
Published: December 30, 2012

dx.doi.org/10.1021/bc300468x | *Bioconjugate Chem.* 2013, 24, 188−195

possessing a gating function with high ligand specificity should be obtained.

With this hope in mind, we constructed a Ca^{2+}-gated artificial channel protein (Rf50-CaMc) using Alm (Rf50) as a transmembrane segment and the C-terminal domain of calmodulin (CaMc) as a Ca^{2+}-sensitive extramembrane segment. Assessment of Rf50-CaMc using the planar lipid-bilayer method, which allows both real-time and single channel measurements, showed Ca^{2+}-induced elongation of the specific channel open state with a resulting increase in the mean channel current. In contrast, Mg^{2+} produced no significant changes in the channel current. An Alm-based Ca^{2+}-gated ion channel was thus successfully created by using a sensing domain derived from a natural protein as an extramembrane segment.

MATERIALS AND METHODS

Peptide and Protein Synthesis. The thioester of Rf50 (**3**) (see Figure 1) was prepared using Fmoc-solid-phase synthesis

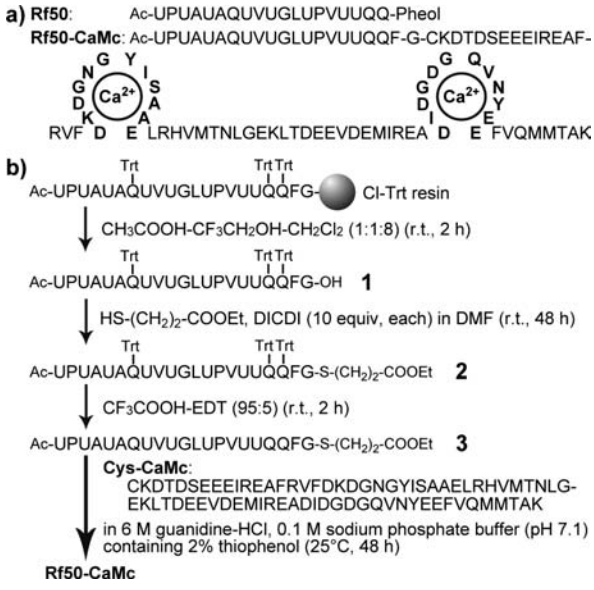

Figure 1. (a) Structure of Rf50 and Rf50-CaMc. Abbreviations: U, Aib; Pheol, phenylalaninol; Ac, acetyl. Two Ca^{2+}-binding loops are highlighted in bold. (b) Synthesis of Rf50-CaMc. Abbreviations: DICDI, diisopropylcarbodiimide; EDT, ethanedithiol; Trt, trityl.

followed by conversion of the carboxyl terminus to the thioester as previously reported.[17] The C-terminal domain of calmodulin (corresponding to the residues 77−148 of calmodulin) bearing a Cys on the N-terminus (Cys-CaMc) was prepared by recombinant expression using intein-mediated purification with an affinity chitin-binding tag (IMPACT) system.[18] Native chemical ligation of thioester **3** with Cys-CaMc yielded the fusion protein Rf50-CaMc. Details about preparation of Rf50-CaMc are described in the Supporting Information.

Circular Dichroism (CD) Measurements. The CD spectra were recorded on a Jasco J-820 spectropolarimeter in 0.15 M KCl, 20 mM 2-(*N*-morpholino)ethanesulfonic acid (MES), 0.2 mM EDTA, 1 mM dithiothreitol (DTT), and 10 μM of CaMc (pH 5.4) at 25 °C in a 0.1 cm path length cell under a nitrogen atmosphere. Each CD spectrum represents an average of 6 scans, obtained at 0.5 nm intervals between 200 and 260 nm with a scanning speed of 100 nm min^{-1}. For preparation of liposomes, a thin film of 1-palmitoyl-2-oleoylphosphatidylcholine (POPC) (NOF corporation, Tokyo, Japan) after drying under vacuum overnight was hydrated with a buffer, and vortex-mixed to produce multilamellar vesicles. The suspension was freeze−thawed for five cycles followed by multiple extrusions (31 times) through a 100 nm pore size polycarbonate membrane using a LiposoFast device (Avestin, Ottawa, Canada) to produce large unilamellar vesicles (LUVs).

Channel Activity Measurements. Planar lipid bilayers were formed from diphytanoylphosphatidylcholine (Avanti, Alabaster, AL, USA) by the monolayer-folding method.[19] A small quantity (usually 1−4 μL) of Rf50 and Rf50-CaMc in ethanol was added to the electrolyte solutions (1 mL) on one side of the membrane (designated as the *cis* side) to obtain each final concentration. $CaCl_2$ or $MgCl_2$ was added from 2 M stock solution in Milli-Q water to both sides of the membrane. A pair of Ag-AgCl electrodes was used for current measurement and voltage supply. The *cis*- and *trans*-side electrodes were connected to a DC voltage source and to the virtual ground of an in-house-made current amplifier, respectively. The output voltages of the current amplifier were recorded with a DL708 8 CH Digital Scope (Yokogawa, Tokyo, Japan) with sampling frequency of 2 kHz after filtering at 0.4 kHz. All channel current records in this study were carried out at *cis*-positive voltage of +180 mV at 25 ± 1 °C.

Conductance histograms were calculated from channel current records for 20 s. Relative frequency was calculated as the highest frequency to be 1 except for Figures 4d and S3a. As

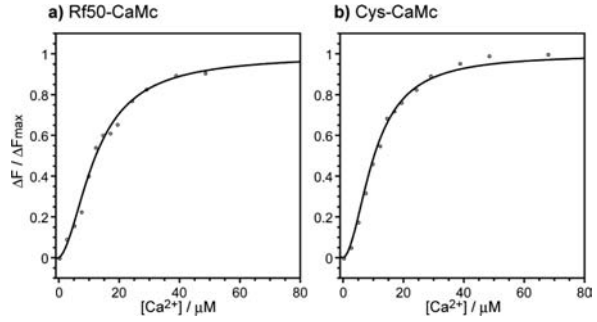

Figure 2. Tyrosine fluorescence measurements of (a) Rf50-CaMc and (b) Cys-CaMc. Representative data from three independent experiments are shown. Solution: 0.15 M KCl containing 20 mM MES, 0.1 mM DTT and 20 μM POPC liposomes (pH 5.4); Rf50-CaMc or Cys-CaMc concentration: 0.4 μM.

for Figures 4d and S3a, channel conductances were not constant and no discrete conductance levels were observed, then the frequency of the closed level (0 nS) was set to be 1.

The mean channel current (see Figures 4c,f, S3c and S4b) was calculated as follows: (1) the mean channel current was calculated from the value of the respective channel current recordings for 1 s; and (2) the averages and standard deviations for a mean channel current of 50 s were obtained.[11]

Tyrosine Fluorescence Measurements. Tyrosine fluorescence emission spectra were monitored at 305 nm with excitation at 275 nm on a RF-5300PC spectrofluorophotometer (Shimadzu, Kyoto, Japan) at 25 °C. The excitation and emission bandwidths were 5 and 15 nm, respectively.

The association constants of Rf50-CaMc and Cys-CaMc for calcium, K_1 and K_2, were calculated according to a stepwise binding scheme.[20] In this analysis, fluorescence change at 305

dx.doi.org/10.1021/bc300468x | Bioconjugate Chem. 2013, 24, 188−195

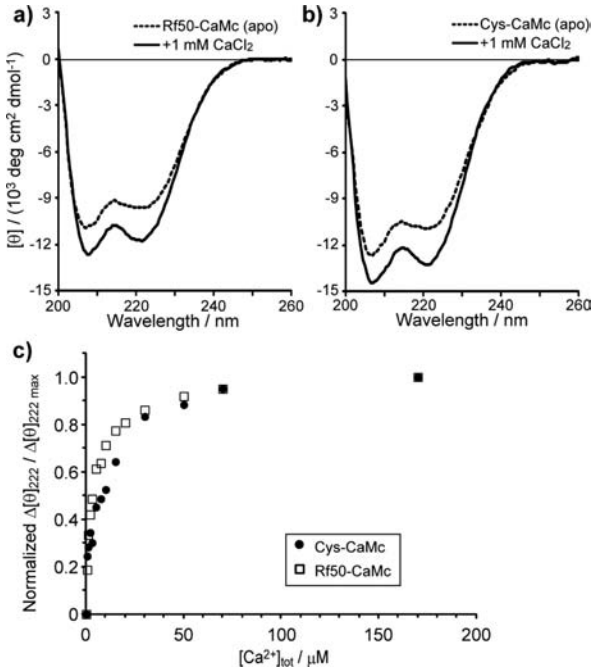

Figure 3. (a, b) Ca^{2+}-dependent folding of (a) Rf50-CaMc and (b) Cys-CaMc in the presence of 0.5 mM POPC liposomes. (c) Normalized $\Delta[\theta]_{222}/\Delta[\theta]_{222\ max}$ was plotted as a function of total calcium concentration $[Ca^{2+}]_{tot}$. The data points represent the average of two experiments. Solution: 0.15 M KCl containing 20 mM MES, 0.2 mM EDTA and 1 mM DTT (pH 5.4) (a, b) or 0.15 M KCl containing 20 mM MES and 1 mM DTT (pH 5.4) (c); Rf50-CaMc or Cys-CaMc concentration: 10 μM (a, b) or 5 μM (c).

nm was assumed to be derived from fractional saturation of two Ca^{2+}-binding loops of proteins, and the contribution to the fluorescence change of each Ca^{2+}-binding loop was assumed to be equal. That is

$$\Delta F/\Delta F_{max} = ([P{\cdot}Ca] + 2[P{\cdot}2Ca])/2[P]_{tot} \quad (1)$$

where ΔF is fluorescence change from apo state, ΔF_{max} is maximum fluorescence change, $[P]_{tot}$ is total protein concentration, and $[P{\cdot}Ca]$ and $[P{\cdot}2Ca]$ are the concentrations of protein of one or two Ca^{2+}-bound form, respectively. On the other hand

$$[P]_{tot} = [P] + [P{\cdot}Ca] + [P{\cdot}2Ca] \quad (2)$$

$$[P{\cdot}Ca] = K_1[P][Ca^{2+}] \quad (3)$$

$$[P{\cdot}2Ca] = K_1K_2[P][Ca^{2+}]^2 \quad (4)$$

where $[P]$ is protein concentration in apo state and $[Ca^{2+}]$ is free calcium concentration. Then, eq 1 can be rewritten as

$$\Delta F/\Delta F_{max} = (K_1[Ca^{2+}] + 2K_1K_2[Ca^{2+}]^2) /2(1 + K_1[Ca^{2+}] + K_1K_2[Ca^{2+}]^2) \quad (5)$$

K_1 and K_2 were obtained by fitting data to eq 5 using the Kaleida Graph program (Abelbeck software). $[Ca^{2+}]$ of each plot was calculated by the following equation:

$$[Ca^{2+}] = [Ca^{2+}]_{tot} - 2[P]_{tot}(\Delta F/\Delta F_{max}) \quad (6)$$

where $[Ca^{2+}]_{tot}$ is total calcium concentration.

ANS Fluorescence Measurements. 8-Anilinonaphthalene-1-sulfonic acid (ANS), ammonium salt was purchased from Sigma-Aldrich (St Louis, MO, USA). ANS fluorescence emission spectra were recorded between 400 and 650 nm with excitation at 385 nm on a Shimadzu RF-5300PC at 25 °C. The excitation and emission bandwidths were 5 nm.

The obtained data plots shown in Figure 5c were analyzed by two different equations. In the range of $[Ca^{2+}] \leq 120$ μM, the data plots were analyzed in the same method used for tyrosine fluorescence measurements. That is, $\Delta\lambda/\Delta\lambda_{max}$ were assumed to be proportional to fractional saturation of Ca^{2+}-binding

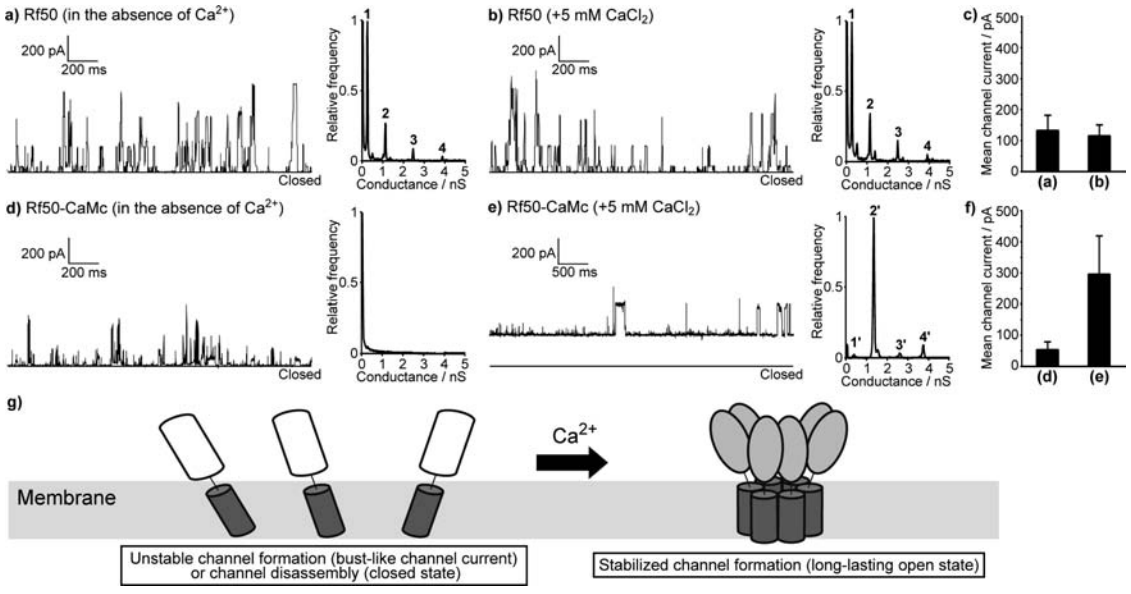

Figure 4. Channel current records and conductance histograms of Rf50 and Rf50-CaMc in the absence (a,d) or presence (b,e) of 5 mM $CaCl_2$, and mean channel current calculated from the records for 50 s (c,f). Voltage: +180 mV; electrolyte: 1 M KCl containing 20 mM MES, 0.2 mM EDTA, and 10 mM DTT (pH 5.4); peptide (protein) concentration: 5 nM (Rf50) or 10 nM (Rf50-CaMc). (g) Schematic representation of Ca^{2+}-stimulated gating of the Rf50-CaMc channel.

dx.doi.org/10.1021/bc300468x | Bioconjugate Chem. 2013, 24, 188−195

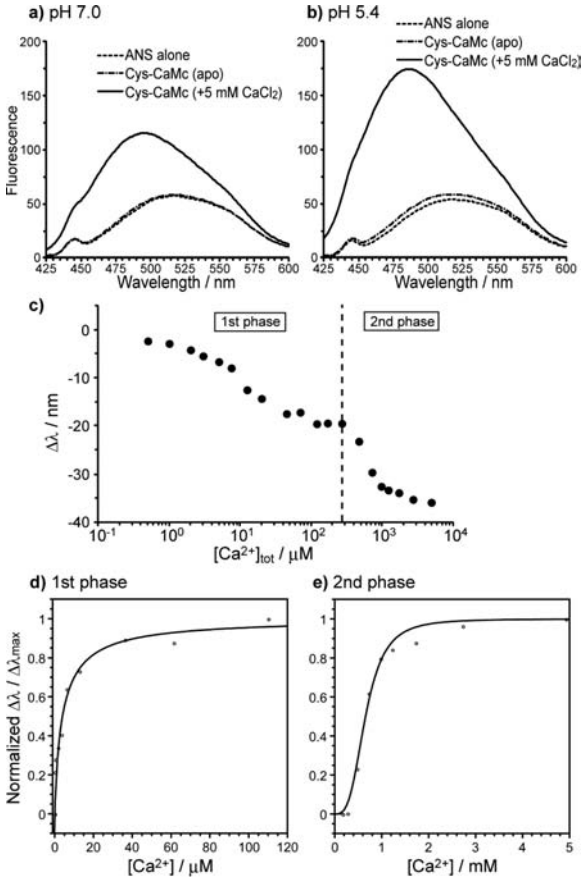

Figure 5. (a,b) ANS binding to Cys-CaMc in the absence or presence of 5 mM $CaCl_2$ at pH 7.0 (a) or pH 5.4 (b). (c) $\Delta\lambda$ plotted as a function of $[Ca^{2+}]_{tot}$ (pH 5.4). (d,e) The plots were divided into two groups and analyzed separately. The plots of each group were normalized to a scale of 0 to 1. The plots of the first group ($[Ca^{2+}]$ of 0−120 μM) were fitted to eq 7 (d), and the plots of the second group ($[Ca^{2+}]$ of 120−5000 μM) were fitted to the Hill equation (eq 9) (e). Solution: 0.15 M KCl containing 20 mM HEPES, 0.2 mM EDTA, and 1 mM DTT (pH 7.0) (a), 0.15 M KCl containing 20 mM MES, 0.2 mM EDTA, and 1 mM DTT (pH 5.4) (b), 0.15 M KCl containing 20 mM MES and 1 mM DTT (pH 5.4) (c−e); ANS concentration: 30 μM; Cys-CaMc concentration: 5 μM.

loops, and the contribution to $\Delta\lambda$ of each Ca^{2+}-binding loop was assumed to be equal.

$$\Delta\lambda/\Delta\lambda_{max} = (K_1[Ca^{2+}] + 2K_1K_2[Ca^{2+}]^2) /2(1 + K_1[Ca^{2+}] + K_1K_2[Ca^{2+}]^2) \quad (7)$$

$$[Ca^{2+}] = [Ca^{2+}]_{tot} - 2[P]_{tot}(\Delta\lambda/\Delta\lambda_{max}) \quad (8)$$

$[Ca^{2+}]$ was calculated by eq 8, and the data plots were fitted to eq 7.

In the range of $[Ca^{2+}] \geq 120$ μM, $\Delta\lambda/\Delta\lambda_{max}$ were fitted by the following Hill equation:

$$[P\cdot(2 + n)Ca]/([P\cdot 2Ca] + [P\cdot(2 + n)Ca]) = [Ca^{2+}]^n/(K_{0.5}{}^n + [Ca^{2+}]^n) \quad (9)$$

where $[P\cdot 2Ca]$ is the concentration of protein of two Ca^{2+}-bound form, $[P\cdot(2+n)Ca]$ is the concentration of protein of further n molecules of Ca^{2+}-bound form, and $K_{0.5}$ is $[Ca^{2+}]$ at which half of proteins are saturated. In this analysis, total calcium concentration was used for $[Ca^{2+}]$.

Fluorescence Resonance Energy Transfer (FRET) Measurements. Alexa 488 was employed as a FRET donor and Alexa 568 as an acceptor. The Cys residue of Rf50-CaMc was modified with each fluorescent label. Details about of the preparation of the Alexa-labeled Rf50-CaMc are described in Supporting Information. Fluorescence emission spectra of Alexa 488 and Alexa 568 were recorded between 510 and 650 nm with excitation at 500 nm on a Shimadzu RF-5300PC at 25 °C. The excitation and emission bandwidths were 1.5 and 5 nm, respectively.

In Figure 6b, total calcium concentration was used for $[Ca^{2+}]$, and the data plots were fitted to eq 9.

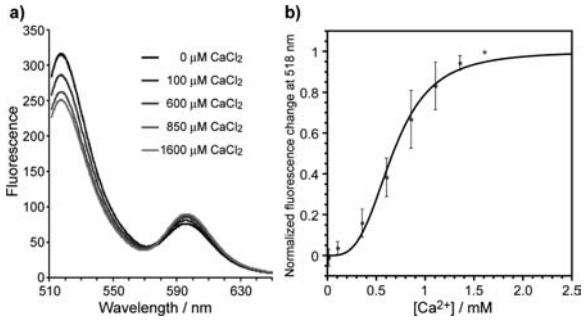

Figure 6. FRET experiments. (a) $CaCl_2$ (100−1600 μM) was added to the solution containing Rf50-CaMc Alexa 488 (0.05 μM) and Rf50-CaMc Alexa 568 (1 μM). Solution: 0.15 M KCl containing 20 mM MES and 50 μM POPC liposomes (pH 5.4). (b) The extent of the decrease of the fluorescence at 518 nm was normalized and plotted as a function of $[Ca^{2+}]$. The data points represent the average of three experiments (±SD). Solution: 0.15 M KCl containing 20 mM MES and 50 μM POPC liposomes (pH 5.4).

RESULTS

Design and Preparation of Rf50-CaMc. We used Rf50 (a non-pH-sensitive component of Alm[19]) as a transmembrane segment and CaMc as a Ca^{2+}-sensitive extramembrane segment (Figure 1a). Alm is a representative channel-forming antimicrobial peptide, and its suitability as a framework for the transmembrane segment of artificial channels has been previously demonstrated.[1,14,15,21] Calmodulin (CaM) is a small, acidic Ca^{2+}-binding protein with a dumbbell-like structure[22] that has been used as a framework for fluorescence-based Ca^{2+} sensing in cells and in vivo.[23,24] CaM is composed of N- and C-terminal domains separated by a central helix linker, and each domain contains two EF-hand Ca^{2+}-binding loops. Upon binding Ca^{2+}, CaM undergoes a structural change so that each pair of EF hands exposes a hydrophobic patch that allows for the binding and activation of numerous target enzymes.[25,26] In addition, there are reports that pH may play a role in the conformation of CaM in solution.[27,28] Isolated N- and C-terminal domains fold independently and bind Ca^{2+}.[29] The C-terminal domain (CaMc) has a higher affinity for Ca^{2+} and induces a greater structural change than the N-terminal domain.[30,31] Thus, we selected CaMc as an extramembrane segment.

Rf50 contains eight α-aminoisobutyric acid (Aib) residues. Aib is an unusual amino acid and the fusion protein Rf50-CaMc cannot be prepared using recombinant techniques. We prepared Rf50-CaMc using native chemical ligation[32] between the Rf50 thioester and the CaMc segment bearing an extra cysteine on the N-terminus (Cys-CaMc) (Figure 1b). Rf50

dx.doi.org/10.1021/bc300468x | Bioconjugate Chem. 2013, 24, 188−195

thioester **3** was prepared using the Fmoc solid-phase method on Cl-Trt resin, as described previously.[17] To facilitate synthesis, the C-terminal phenylalaninol (Pheol) was changed to phenylalanine. After peptide chain construction on the resin and N-terminal acetylation, the protected peptide segment was treated with $CH_3COOH-CF_3CH_2OH-CH_2Cl_2$ (1:1:8) at room temperature for 2 h to detach it from the resin, which yielded **1**. Next, **1** was treated with HS-$(CH_2)_2$−COOEt and diisopropylcarbodiimide (DICDI) (10 equiv each) in dimethylformamide (DMF) at room temperature for 48 h to yield the corresponding thioester **2**. Deprotection of **2** using CF_3COOH−ethanedithiol (EDT) (95:5) at room temperature for 2 h and subsequent high-performance liquid chromatography (HPLC) purification yielded **3** (13% yield from the starting resin). Cys-CaMc was prepared by recombinant expression using intein-mediated purification with an affinity chitin-binding tag (IMPACT) system.[18] Detailed procedures are provided in Supporting Information. Ligation of **3** and Cys-CaMc was conducted in 0.1 M sodium phosphate buffer (pH 7.1) containing 6 M guanidine-HCl and 2% thiophenol at 25 °C for 48 h using 1.7 equiv of **3** to Cys-CaMc. The subsequent HPLC purification yielded a highly pure Rf50-CaMc [32% yield in ligation; matrix-assisted laser desorption/ionization time-of-flight mass spectrometry (MALDI-TOF MS): 10397.5 $(M+H)^+$ (calculated 10397.4)] (see Figure S1 in Supporting Information).

Since the N-terminal region of the CaMc segment (which is proximal to the transmembrane Rf50 segment) is rich in the acidic amino acids Asp and Glu, electrostatic repulsion may prevent Rf50-CaMc from self-assembling in membranes to form channels. To reduce the negative charges, we performed the channel current recording of Rf50-CaMc under acidic conditions (pH 5.4).[27,28]

Ca^{2+}-Induced Conformational Change in the Extramembrane Segment. Prior to measuring the channel current, we confirmed Ca^{2+} binding and Ca^{2+}-induced conformational change in the extramembrane CaMc segment of Rf50-CaMc by measuring the intrinsic tyrosine fluorescence and the CD spectra in the presence of POPC liposomes, respectively (Figures 2 and 3).

Tyrosine fluorescence has been used to monitor Ca^{2+}-binding to CaM.[20] As Figure 2 shows, addition of Ca^{2+} increased the fluorescence intensity of tyrosine of Rf50-CaMc as well as CaMc. The data plots were fitted to eq 5 to yield the following association constants: $K_1 = (2.62 \pm 0.80) \times 10^5\ M^{-1}$ and $K_2 = (2.91 \pm 0.95) \times 10^4\ M^{-1}$ for Rf50-CaMc, and $K_1 = (4.69 \pm 1.81) \times 10^5\ M^{-1}$ and $K_2 = (2.48 \pm 1.03) \times 10^4\ M^{-1}$ for Cys-CaMc that corresponds to the extramembrane segment of Rf50-CaMc. The obtained values are comparable with those previously reported,[20,31] suggesting that the attachment of the Rf50 segment to CaMc segment has no significant effect on the Ca^{2+}-binding to CaMc.

Figure 3 shows the results of CD measurements. In the absence of Ca^{2+}, Rf50-CaMc yielded a spectrum with local minima at 208 and 222 nm, indicative of a helical structure. A significant increase in $[\theta]_{222}$ was observed for Rf50-CaMc in the presence of 1 mM $CaCl_2$ ($[\theta]_{222}$ of -0.96×10^4 and -1.17×10^4 deg cm^2 dmol^{-1} in the absence and presence of 1 mM $CaCl_2$, respectively) (Figure 3a). Similarly, addition of 1 mM $CaCl_2$ increased $[\theta]_{222}$ in the CD spectrum of Cys-CaMc ($[\theta]_{222}$ of -1.08×10^4 and -1.32×10^4 deg cm^2 dmol^{-1} in the absence and presence of 1 mM $CaCl_2$, respectively) (Figure 3b). Figure 3c shows the result of Ca^{2+} titration experiments. A significant Ca^{2+}-dependent increase in $[\theta]_{222}$ of Cys-CaMc was observed up to total calcium concentration of ∼70 μM and this looks to be in accord with the modes of Ca^{2+} binding to the Cys-CaMc segment (Figure 2b). A similar result was obtained for Rf50-CaMc (Figure 3c). These results suggest that the addition of Ca^{2+} induces a conformational change in Cys-CaMc[33] even in the presence of liposomes and that the attachment to the transmembrane segment (Rf50 segment) did not yield significant effects on Ca^{2+}-binding or Ca^{2+}-induced conformational change of the CaMc segment. Additionally, no marked increase in $[\theta]_{222}$ was observed by further addition of Ca^{2+} (up to 5 mM) (Figure S2).

Ca^{2+}-Stimulated Gating of the Rf50-CaMc Channel. The Rf50 and Rf50-CaMc channel currents were measured using the planar lipid bilayer method,[19] which is as sensitive as the patch-clamp method (Figure 4). When Rf50 was added to the *cis* side of the membrane, multiple conductance levels (or open states) were observed at a *cis*-positive voltage (+180 mV), which is typical for Alm analogues (Figure 4a). This suggests that there are open states of various pore sizes with different association numbers in the lipid bilayer.[34] The frequent transition between conductance levels is thought to reflect the uptake and release of Rf50 molecules into and from the channel. As shown in Figure 4a, level 1 (0.26 nS) was most frequent and 3-fold more common than level 2 (1.1 nS). Addition of Ca^{2+} did not change the channel duration time, conductance histogram (Figure 4b), or mean channel current (Figure 4c). On the other hand, Ca^{2+} had a significant effect on Rf50-CaMc (Figure 4d−f). In the absence of Ca^{2+}, Rf50-CaMc yielded burst-like channel currents with no discrete channel conductance levels (Figure 4d). However, the addition of Ca^{2+} significantly increased the duration of level 2′ (1.3 nS), which was >30 times more frequent than level 1′ (0.38 nS) (Figure 4e). According to a study using covalently tethered Alm dimers,[35] level 2′ corresponds to 6-mer assembly of Rf50 molecules. As a result, addition of Ca^{2+} produced an approximately 6-fold increase in mean channel current (Figure 4f). Thus, we successfully created a Ca^{2+}-gated artificial channel protein that utilizes a conformational change for channel gating.

Mechanism of Ca^{2+}-Stimulated Gating. Ca^{2+}-induced assembly stabilization was also observed at pH 7.0, accompanied by a less prominent stabilization of the open state 2″ (corresponding to level 2′ at pH 5.4) (Figure S3b). The mechanism behind Ca^{2+} induction of a stable channel assembly at pH 5.4 is currently unclear. However, it is possible that steric hindrance between the extramembrane segments plays a role in channel peptide assembly.[15] Here, steric hindrance of the CaMc segments on the membrane surface in the absence of Ca^{2+} may prevent the Rf50 segment from self-assembling in the membrane, yielding burst-like current or frequent channel closing. On the other hand, if exposure of the hydrophobic interiors of the CaMc segment induced by Ca^{2+} reduces steric hindrance or stabilizes a specific association state through hydrophobic interactions between the CaMc segments, this may favorably stabilize open state 2′ (Figure 4g). Finn et al. also confirmed the Ca^{2+}-induced exposure of hydrophobic residues of CaM C-terminal domain, by comparing the solution structures of the apo and Ca^{2+}-bound forms using NMR spectroscopy.[33]

To support this hypothesis, changes in the surface hydrophobicity of the CaMc segment induced by Ca^{2+} were ascertained using ANS fluorescent measurement. ANS is a fluorescent probe and is commonly used to monitor conforma-

dx.doi.org/10.1021/bc300468x | *Bioconjugate Chem.* 2013, 24, 188−195

tional changes in proteins, including Ca^{2+}-binding proteins.[20,36] Excitation of unbound ANS at 385 nm results in a low fluorescent emission with a maximum around 520 nm. When ANS binds to hydrophobic regions of proteins, the fluorescence spectrum is blue-shifted with a maximum around 480 nm and emission intensity is increased. The effects of Ca^{2+} and pH on ANS fluorescence were examined for Cys-CaMc (Figure 5). As expected, the apo state of Cys-CaMc showed only negligible binding of ANS regardless of pH. On the other hand, ANS bound strongly to Ca^{2+}-loaded Cys-CaMc, which is seen as a blue shift (24 nm, from 519 to 495 nm) with an approximately 2-fold enhancement of fluorescence at pH 7.0 (Figure 5a). In contrast, a more significant blue shift (33 nm, from 519 to 486 nm) with an approximately 3-fold enhancement of fluorescence was observed at pH 5.4 (Figure 5b). This suggests that Ca^{2+}-binding induces a conformational change in Cys-CaMc so that hydrophobic residues buried in the apo-form become exposed to the solvent.[20,25,26,33,36,37] In addition, the extent of surface hydrophobicity in the presence of Ca^{2+} at pH 5.4 is higher than that at pH 7.0. This may alter Rf50-CaMc channel stability, which is reflected in the relative frequency of level 2′ and 2″ (Figures 4e and S3b).

Ca^{2+} titration study at pH 5.4 was then conducted using ANS (Figure 5c). Two obvious plateau phases were observed in the plot of the Ca^{2+}-induced wavelength shift ($\Delta\lambda$) in fluorescence intensity maxima from that in the absence of calcium. The first plateau phase appeared at the total calcium concentration of ~70 μM, where the saturation of tyrosine fluorescence and $\Delta[\theta]_{222}$ was observed (Figures 2b and 3c). The normalized $\Delta\lambda/\Delta\lambda_{max}$ was plotted as a function of $[Ca^{2+}]$ up to 120 μM and fitted by eq 7 as well as Figure 2 to yield the following association constants: $K_1 = 5.98 \times 10^5\ M^{-1}$ and $K_2 = 1.05 \times 10^5\ M^{-1}$ (Figure 5d). The value for K_2 was about 4 times larger than that obtained using tyrosine fluorescence, while the value for K_1 was comparable (Figure 2b). This might be due to the difference in methods of analysis.

Increment in total calcium concentration produced no significant blue shift up to 270 μM for Cys-CaMc. However, further addition of Ca^{2+} resulted in induction of a marked blue shift, yielding the second plateau phase appearing at the Ca^{2+} concentration of ~2 mM. Considering that this second plateau phase was not observed in the CD measurement (Figure S2), this suggests that Cys-CaMc forms its secondary/tertiary structure by the Ca^{2+} binding to its two Ca^{2+}-binding loops at the first plateau phase, and then induces further structural alteration, presumably leading to association of Cys-CaMc molecules at the second plateau phase. Assuming that the binding of further n molecules of calcium occurred at the second plateau phase, the normalized $\Delta\lambda/\Delta\lambda_{max}$ was plotted as a function of $[Ca^{2+}]$ from 120 μM to 5 mM and fitted by the Hill equation (eq 9) to yield the following values: $n = 3.23$ and $K_{0.5} = 657$ μM (Figure 5e).

Fluorescent Resonance Energy Transfer (FRET) Experiment. The Ca^{2+}-induced association of Rf50-CaMc was then confirmed by FRET experiment. Alexa 488-labeled Rf50-CaMc and Alexa 568-labeled Rf50-CaMc were prepared as the FRET donor and acceptor, respectively. The Alexa-labeling was conducted onto the Cys residue used for native ligation to produce Rf50-CaMc.

Figure 6a shows the change of fluorescent emission spectra by the addition of $CaCl_2$ (100−1600 μM) to the solution which contains Rf50-CaMc Alexa 488 and Rf50-CaMc Alexa 568 in the presence of POPC liposomes. No significant change in spectra was observed up to $[Ca^{2+}]$ of 300 μM. When $[Ca^{2+}]$ exceeded this, a significant decrease in Alexa 488 fluorescence (maximum at 518 nm) together with increase in Alexa 568 was observed, indicating the association of Rf50-CaMc moleucles. Note that the blue shift in the ANS fluorescent measurement (Figure 4c) was observed at the same $[Ca^{2+}]$ range, suggesting that the exposure of hydrophobic moieties on the CaMc segment stimulate the association of the channel proteins. The decrease in fluorescence at 518 nm was plotted as a function of $[Ca^{2+}]$, and a sigmoidal data plot reminiscent of Figure 5e was obtained (Figure 6b). The plots were fitted by the Hill equation (eq 9) to yield the following values: $n = 3.61 \pm 0.98$ and $K_{0.5} = 676 \pm 89$ μM. The values were very close to those obtained from ANS fluorescence study, which indicates the association among Rf50-CaMc proteins is parallel to the exposed hydrophobicity of the extramembrane CaMc segment.

Specificity of Rf50-CaMc to Ca^{2+}. By employing the natural protein segment that specifically binds Ca^{2+}, Rf50-CaMc should maintain high specificity to Ca^{2+} over other cations. In support of this, there was no detectable effect on channel conductance and mean channel current of Rf50-CaMc in the presence of Mg^{2+} (Figure S4) as compared with Rf50-CaMc in the absence of metals (Figure 4d). As described above, the Ca^{2+}-specific gating of Rf50-CaMc may be explained by exposure of the hydrophobic interface in the CaMc segment following Ca^{2+} binding. This was confirmed using ANS fluorescent measurements in the presence of Mg^{2+} (Figure S5). As expected, the addition of Mg^{2+} to Cys-CaMc did not induce significant shifts in the fluorescence spectrum nor enhance the emission intensity, which suggests that Mg^{2+} does not induce the exposure of CaMc hydrophobic residues.

DISCUSSION

In this study, we used native chemical ligation to conjugate Rf50 (as a transmembrane segment) and CaMc (as an extramembrane segment), creating an artificial ion channel that transmits conformational changes in the extramembrane segment and alters the channel current level upon induction by Ca^{2+} binding. The addition of Ca^{2+} at pH 5.4 significantly stabilized the channel open state (corresponding to a 6-mer assembly) and increased the mean channel current by 6-fold, while Mg^{2+} produced no significant changes in the channel current. The ANS fluorescent measurement revealed that surface hydrophobicity of the extramembrane segment was increased by Ca^{2+}, but was not influenced by Mg^{2+}, suggesting that Ca^{2+}-induced channel stabilization may be related to an increased surface hydrophobicity of the extramembrane segment.

The strength of Alm-based approaches in the design of artificial ion channels should be the feasibility of attaining channel function based on a simple peptide assembly together with possible employment of chemical methods to construct channels bearing unnatural amino acids or functional groups that are not equipped in natural proteins. It has been previously demonstrated that coupling of a ligand binding moiety to Alm confers ligand modulation. However, the gating function of these designed channels was, in general, not highly optimized.

Utilization of natural protein motifs specific to intrinsic ligands as an extramembrane segment should be an alternative approach in improving channel function of Alm-based channels. In the present study, we prepared Rf50-CaMc via native chemical ligation of chemically synthesized Alm segment with CaMc segment prepared by the recombinant technique, and

dx.doi.org/10.1021/bc300468x | Bioconjugate Chem. 2013, 24, 188−195

successful gating of the channel by Ca^{2+} was accomplished. These segments exerted their functions (Ca^{2+}-responsive structural switch and pore formation) without hampering the structure and function of each other. From the studies using tyrosine fluorescence and CD spectroscopy, the CaMc segment was suggested to form its secondary/tertiary structure by the addition of Ca^{2+} in the presence of liposomes, regardless of the conjugation with transmembrane Rf50 segment. This structural alteration was almost completed at total calcium concentration of ~70 μM. Further increase in calcium concentration (>270 μM), however, yielded a second phase of structural alteration: Significant increase in FRET efficiency among Alexa 488- and Alexa 568-labeled Rf50-CaMc was observed together with ANS binding to Cys-CaMc segment. Since there was no marked increase in helical content, analyzed by $[\theta]_{222}$, the structural alteration in this second phase was assumed due to the interaction among the prefolded CaMc segment, leading to stabilization of Rf50-CaMc channel assembly. It would be especially interesting that the hydrophobic interaction among extramembrane CaMc segments plays an important role in forming a metastable assembly (presumably of 6 mer) of Rf50-CaMc. Thus, this study has implications not only on the construction of artificial channels having gating functions but also on the methods of structural formation of membrane proteins.

We have previously reported a hybrid channel peptide of Alm and leucine-zipper segment, where Fe(III)-stimulated decrease in helical structure of the extramembrane leucine-zipper segment diminishes the interaction among the extramembrane segments and leads to opening of the channel.[15] In contrast, Rf50-CaMc in this study stabilized the open channel structure by strengthening the interaction among the extramembrane CaMc segments. Therefore, although both our previous study of the Alm-leucine-zipper-based Fe(III) channel and this study share the concept of implanting an extramembrane segment onto the Alm segment, their gating mechanisms should be different. This study thus added the flexibility in the design of gating functions in these artificial channels.

Ohndorf and MacKinnon reported that addition of a prokaryotic cyclic nucleotide-binding domain endowed KcsA-derived potassium channel with cyclic nucleotide-gating function.[38] This hybrid channel, however, employed a whole cyclic nucleotide-binding domain fused with KcsA channel composed of four transmembrane domains (molecular mass, ~33 kDa). Our intention in this study is to produce a channel protein which mimics the function of natural channel proteins with the simplest possible structure, and this would be beneficial for the application to artificial sensors/devices as well as artificial cellular gates in synthetic biology. Thus, successful employment of a natural protein motif as the extramembrane gating segment for Alm, while maintaining the simple structure together with intrinsic functions of extramembrane and channel-forming segments, should also be the impact of the present study.

We should also note that certain care may be needed to choose the suitable extramembrane segment and assay condition, considering that a less marked increase in Alm-CaMc channel current was observed by the addition of Ca^{2+} at pH 7.0 than at pH 5.4, presumably due to the possible repulsion of acidic amino acids in the connecting region of CaMc to the Alm segment that prevent channel assembly formation. Similar behavior is observed for Alm pyromellitate (Alm-PM) bearing three negative charges on the C-terminus.[12] An alternative explanation may lie in the repulsions between the CaMc segments. It is known that the more compact forms of full length of CaM may be encouraged by lowering the pH.[27,39] This is probably due to the high number of charged residues distributed on the surface of CaM to yield repulsions between its two lobes at neutral pH, which is partially lost at pH 5.4.

Although further efforts are required to create artificial channels with more sophisticated functions, current data strongly suggest the promise of our approach using a structural switch in the extramembrane segment for channel gating to develop novel ion channel-based sensing systems. Employment of a microfluidic system based on planar lipid bilayer methods[40,41] may also enhance the applicability of these channel systems as molecular sensors or high-throughput screening systems.

■ ASSOCIATED CONTENT

Ⓢ Supporting Information

Details about synthesis of Rf50, Cys-CaMc, Rf50-CaMc and Alexa-labeled Rf50-CaMc, and five figures. This material is available free of charge via the Internet at http://pubs.acs.org.

■ AUTHOR INFORMATION

Corresponding Author

*Tel.: +81-774-38-3210; Fax: +81-774-32-3038; E-mail: futaki@scl.kyoto-u.ac.jp.

Notes

The authors declare no competing financial interest.

■ ACKNOWLEDGMENTS

This work was supported by Grants-in-Aid for Scientific Research from the Ministry of Education, Culture, Sports, Science and Technology of Japan. D. N. received a JSPS Research Fellowship for Young Scientists.

■ REFERENCES

(1) Majd, S., Yusko, E. C., Billeh, Y. N., Macrae, M. X., Yang, J., and Mayer, M. (2010) Applications of biological pores in nanomedicine, sensing, and nanoelectronics. *Curr. Opin. Biotechnol. 21*, 439−76.

(2) Bayley, H., and Jayasinghe, L. (2004) Functional engineered channels and pores (Review). *Mol. Membr. Biol. 21*, 209−20.

(3) Matile, S., Jentzsch, A. V., Montenegro, J., and Fin, A. (2011) Recent synthetic transport systems. *Chem. Soc. Rev. 40*, 2453−74.

(4) Maglia, G., Heron, A. J., Stoddart, D., Japrung, D., and Bayley, H. (2010) Analysis of single nucleic acid molecules with protein nanopores. *Methods Enzymol. 475*, 591−623.

(5) Futaki, S. (1998) Peptide ion channels: design and creation of function. *Biopolymers 47*, 75−81.

(6) Futaki, S., and Asami, K. (2007) Ligand-induced extramembrane conformation switch controlling alamethicin assembly and the channel current. *Chem. Biodivers. 4*, 1313−22.

(7) Berridge, M. J., Lipp, P., and Bootman, M. D. (2000) The versatility and universality of calcium signalling. *Nat. Rev. Mol. Cell Biol. 1*, 11−21.

(8) Berridge, M. J., Bootman, M. D., and Roderick, H. L. (2003) Calcium signalling: dynamics, homeostasis and remodelling. *Nat. Rev. Mol. Cell Biol. 4*, 517−29.

(9) Zhang, Y., Ruder, W. C., and LeDuc, P. R. (2008) Artificial cells: building bioinspired systems using small-scale biology. *Trends Biotechnol. 26*, 14−20.

(10) Leitgeb, B., Szekeres, A., Manczinger, L., Vágvölgyi, C., and Kredics, L. (2007) The history of alamethicin: a review of the most extensively studied peptaibol. *Chem. Biodivers. 4*, 1027−51.

(11) Noshiro, D., Asami, K., and Futaki, S. (2010) Metal-assisted channel stabilization: disposition of a single histidine on the N-terminus of alamethicin yields channels with extraordinarily long lifetimes. *Biophys. J. 98*, 1801−8.
(12) Woolley, G. A., Epand, R. M., Kerr, I. D., Sansom, M. S. P., and Wallace, B. A. (1994) Alamethicin pyromellitate: an ion-activated channel-forming peptide. *Biochemistry 33*, 6850−8.
(13) Woolley, G. A., and Lougheed, T. (2003) Modeling ion channel regulation. *Curr. Opin. Chem. Biol. 7*, 710−4.
(14) Futaki, S., Fukuda, M., Omote, M., Yamauchi, K., Yagami, T., Niwa, M., and Sugiura, Y. (2001) Alamethicin-leucine zipper hybrid peptide: a prototype for the design of artificial receptors and ion channels. *J. Am. Chem. Soc. 123*, 12127−34.
(15) Kiwada, T., Sonomura, K., Sugiura, Y., Asami, K., and Futaki, S. (2006) Transmission of extramembrane conformational change into current: construction of metal-gated ion channel. *J. Am. Chem. Soc. 128*, 6010−1.
(16) Jiang, Y., Lee, A., Chen, J., Cadene, M., Chait, B. T., and MacKinnon, R. (2002) Crystal structure and mechanism of a calcium-gated potassium channel. *Nature 417*, 515−22.
(17) Futaki, S., Sogawa, K., Maruyama, J., Asahara, T., Niwa, M., and Hojo, H. (1997) Preparation of peptide thioesters using Fmoc-solid-phase peptide synthesis and its application to the construction of a template-assembled synthetic protein (TASP). *Tetrahedron Lett. 38*, 6237−40.
(18) Xu, M. Q., and Evans, T. C., Jr. (2001) Intein-mediated ligation and cyclization of expressed proteins. *Methods 24*, 257−77.
(19) Asami, K., Okazaki, T., Nagai, Y., and Nagaoka, Y. (2002) Modifications of alamethicin ion channels by substitution of Glu-7 for Gln-7. *Biophys. J. 83*, 219−28.
(20) Tsuruta, H., and Sano, T. (1990) A fluorescence temperature-jump study on Ca^{2+}-induced conformational changes in calmodulin. *Biophys. Chem. 35*, 75−84.
(21) Zhang, Y., Futaki, S., Kiwada, T., and Sugiura, Y. (2002) Detection of protein-ligand interaction on the membranes using C-terminus biotin-tagged alamethicin. *Bioorg. Med. Chem. 10*, 2635−9.
(22) Babu, Y. S., Sack, J. S., Greenhough, T. J., Bugg, C. E., Means, A. R., and Cook, W. J. (1985) Three-dimensional structure of calmodulin. *Nature 315*, 37−40.
(23) Miyawaki, A., Llopis, J., Heim, R., McCaffery, J. M., Adams, J. A., Ikura, M., and Tsien, R. Y. (1997) Fluorescent indicators for Ca^{2+} based on green fluorescent proteins and calmodulin. *Nature 388*, 882−7.
(24) Wallace, D. J., Meyer zum Alten Borgloh, S., Astori, S., Yang, Y., Bausen, M., Kügler, S., Palmer, A. E., Tsien, R. Y., Sprengel, R., Kerr, J. N. D., Denk, W., and Hasan, M. T. (2008) Single-spike detection *in vitro* and *in vivo* with a genetic Ca^{2+} sensor. *Nat. Methods 5*, 797−804.
(25) Johnson, J. D., and Wittenauer, L. A. (1983) A fluorescent calmodulin that reports the binding of hydrophobic inhibitory ligands. *Biochem. J. 211*, 473−9.
(26) Wriggers, W., Mehler, E., Pitici, F., Weinstein, H., and Schulten, K. (1998) Structure and dynamics of calmodulin in solution. *Biophys. J. 74*, 1622−39.
(27) Slaughter, B. D., Unruh, J. R., Allen, M. W., Bieber Urbauer, R. J., and Johnson, C. K. (2005) Conformational substates of calmodulin revealed by single-pair fluorescence resonance energy transfer: influence of solution conditions and oxidative modification. *Biochemistry 44*, 3694−707.
(28) Isvoran, A., Craescu, C. T., and Alexov, E. (2007) Electrostatic control of the overall shape of calmodulin: numerical calculations. *Eur. Biophys. J. 36*, 225−37.
(29) Barth, A., Martin, S. R., and Bayley, P. M. (1998) Specificity and symmetry in the interaction of calmodulin domains with the skeletal muscle myosin light chain kinase target sequence. *J. Biol. Chem. 273*, 2174−83.
(30) Martin, S. R., and Bayley, P. M. (1986) The effects of Ca^{2+} and Cd^{2+} on the secondary and tertiary structure of bovine testis calmodulin. A circular-dichroism study. *Biochem. J. 238*, 485−90.
(31) Linse, S., Helmersson, A., and Forsén, S. (1991) Calcium binding to calmodulin and its globular domains. *J. Biol. Chem. 266*, 8050−9.
(32) Dawson, P. E., Muir, T. W., Clark-Lewis, I., and Kent, S. B. H. (1994) Synthesis of proteins by native chemical ligation. *Science 266*, 776−9.
(33) Finn, B. E., Evenäs, J., Drakenberg, T., Waltho, J. P., Thulin, E., and Forsén, S. (1995) Calcium-induced structural changes and domain autonomy in calmodulin. *Nat. Struct. Biol. 2*, 777−83.
(34) Woolley, G. A. (2007) Channel-forming activity of alamethicin: effects of covalent tethering. *Chem. Biodivers. 4*, 1323−37.
(35) Okazaki, T., Sakoh, M., Nagaoka, Y., and Asami, K. (2003) Ion channels of alamethicin dimer N-terminally linked by disulfide bond. *Biophys. J. 85*, 267−73.
(36) Berggård, T., Silow, M., Thulin, E., and Linse, S. (2000) Ca^{2+}- and H^{+}-dependent conformational changes of calbindin D_{28k}. *Biochemistry 39*, 6864−73.
(37) Schauer-Vukasinovic, V., Cullen, L., and Daunert, S. (1997) Rational design of a calcium sensing system based on induced conformational changes of calmodulin. *J. Am. Chem. Soc. 119*, 11102−3.
(38) Ohndorf, U. M., and MacKinnon, R. (2005) Construction of a cyclic nucleotide-gated KcsA K^{+} channel. *J. Mol. Biol. 350*, 857−65.
(39) Negi, S., Aykut, A. O., Atilgan, A. R., and Atilgan, C. (2012) Calmodulin readily switches conformation upon protonating high pK_a acidic residues. *J. Phys. Chem. B 116*, 7145−53.
(40) Bayley, H., Cronin, B., Heron, A., Holden, M. A., Hwang, W. L., Syeda, R., Thompson, J., and Wallace, M. (2008) Droplet interface bilayers. *Mol. Biosyst. 4*, 1191−208.
(41) Le Pioufle, B., Suzuki, H., Tabata, K. V., Noji, H., and Takeuchi, S. (2008) Lipid bilayer microarray for parallel recording of transmembrane ion currents. *Anal. Chem. 80*, 328−32.

NOTE ADDED AFTER ASAP PUBLICATION

This paper was published on the Web on Jan 14, 2013, with the incorrect Supporting Information file. The corrected version was reposted on Jan 15, 2013.